Observation of the Decrease of Larmor Tunneling Times with Lower Incident Energy

David C. Spierings* and Aephraim M. Steinberg†
Centre for Quantum Information and Quantum Control, Department of Physics, University of Toronto, 60 St. George Street, Toronto, Ontario M5S 1A7, Canada
Canadian Institute for Advanced Research, MaRS Centre, West Tower 661 University Ave., Toronto, Ontario M5G 1M1, Canada

(Received 1 February 2021; accepted 12 July 2021; published 20 September 2021; corrected 28 October 2021)

How much time does a tunneling particle spend in a barrier? A Larmor clock, one proposal to answer this question, measures the interaction between the particle and the barrier region using an auxiliary degree of freedom of the particle to clock the dwell time inside the barrier. We report on precise Larmor time measurements of ultracold ^{87}Rb atoms tunneling through an optical barrier, which confirm longstanding predictions of tunneling times. We observe that atoms generally spend less time tunneling through higher barriers and that this time decreases for lower energy particles. For the lowest measured incident energy, at least 90% of transmitted atoms tunneled through the barrier, spending an average of 0.59 ± 0.02 ms inside. This is 0.11 ± 0.03 ms faster than atoms traversing the same barrier with energy close to the barrier's peak and 0.21 ± 0.03 ms faster than when the atoms traverse a barrier with 23% less energy.

DOI: 10.1103/PhysRevLett.127.133001

Tunneling is one of the most famous quantum phenomena and plays a central role in many physical contexts. Despite its ubiquity, certain aspects of tunneling remain enigmatic. How much time does tunneling take? This has been a provocative question for decades, not only because no definitive answer has emerged but also because there is no consensus on a definition for this time [1–3]. Classical intuition would lead one to believe that numerous measures of time should probe the same quantity. Yet, the lack of definite trajectories in quantum mechanics causes seemingly equivalent approaches to yield strikingly different results. The continued work on tunneling times is thus not motivated by the search for a unique timescale but rather by the hope that a few useful and physically significant definitions can be distilled from the countless proposals and their relationships made clear. We emphasize in particular the distinction between two categories of tunneling time definitions: "arrival" and "interaction" times.

Arrival times seek to determine the moment at which a transmitted particle emerges on the far side of a barrier. Early work on the tunneling time problem focused on calculating the group delay, which tracks a wave packet's peak and can be superluminal or even negative [4–7] without violating relativistic causality [3,8]. More recently, the "attoclock" has been demonstrated as a means of measuring the arrival time of an electron escaping from a bound state of the atom's Coulomb potential [9]. There, the rotating polarization of an ionizing pulse provides a kick to the freed electron, thereby encoding the exit time of the tunneling electron in its final momentum. By comparing the exit time to the instant the electric field reaches its maximum, when the ionization probability also reaches its peak, a tunneling delay can be extracted. While a recent measurement [10,11] demonstrates no appreciable delay in the tunneling process, other experiments [12–14] report nonzero delays that remain unexplained [15–18].

Interaction times strive instead to describe how much time a particle *spends* inside the barrier region. Here, we consider the Larmor clock [19,20]. Early measurements of Larmor times for tunneling particles include work in analog optical systems [21,22] and with neutrons [23]. Recently, we made a Larmor time measurement [24] with ultracold atoms that disentangled the nonzero time spent inside the barrier from the backaction of the measurement. These results constituted an important milestone but were severely limited by systematic errors as large as 40% of the measured times as well as uncertain effective temperatures of the incident wave packet, 2 ± 1 nK, which meant that the portion of transmission due to tunneling may have only been a small minority.

Here, we report new Larmor time measurements with systematic errors reduced to typically 4% of the measured values and with lower-temperature, stable wave packet preparation, 1.3 ± 0.2 nK. In addition, thanks to more sensitive imaging capable of reliably counting tens of atoms (another order of magnitude improvement), we can now observe transmission at energies such that tunneling is the dominant means of passage through the barrier. We observe that the time particles spend interacting with the barrier decreases with their energy below it, while the backaction grows. This is observable only because a large majority of atoms tunnel through the barrier for the lowest measured energies. Furthermore, we demonstrate that particles spend less time tunneling through a higher barrier.

A Larmor clock uses an auxiliary degree of freedom of the tunneling particle to measure the dwell time inside the barrier. The dwell time is simply the probability of finding a

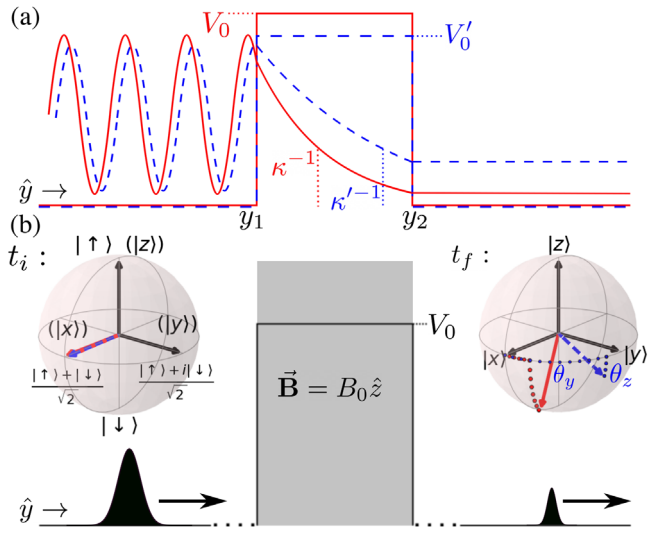

FIG. 1. (a) Illustrations of $|\psi(y)|^2$ for a wave of energy E incident on square barriers of two heights. The dwell time in the red (solid) scenario, with a higher barrier, is lower than in the blue (dashed) case, with a lower barrier. (b) The standard Larmor experiment starts with a spin-1/2 particle (here an electron), polarized along the x axis, incident on a square barrier. A magnetic field, localized to the barrier region and pointing along the z axis, causes the spin to precess while in the barrier. The angles of precession θ_y and alignment θ_z of the transmitted wave packet determine the Larmor tunneling times when the energy of the wave packet is below the barrier. The right Bloch sphere illustrates the rotations resulting from a Larmor measurement of the scenarios shown in (a).

particle in a region integrated over all times, which in one dimension is given by

$$\tau_d = \int_{-\infty}^{\infty} dt \int_{y_1}^{y_2} dy |\psi(y,t)|^2 \equiv \int_{-\infty}^{\infty} dt \langle\psi|\Theta_d|\psi\rangle, \quad (1)$$

where y_1 and y_2 are the boundaries of the region of interest, $\Theta_d \equiv \int_{y_1}^{y_2} dy|y\rangle\langle y|$ is a projector onto the barrier region, and $\psi(y,t)$ is the wave function. The dwell time is a clear-cut definition of the time spent in a region for any probabilistic evolution but, in the case of tunneling, does not distinguish between reflected and transmitted subensembles. A Larmor clock implements a measurement of time conditioned on transmission or reflection by having the measuring device carried by each particle and arranging the measurement interaction so that it does not significantly affect the motion [25].

The paradigmatic Larmor experiment considers an ensemble of spin-1/2 particles incident on a barrier as illustrated in Fig. 1(b), drawn for an electron. Before interacting with the barrier, each particle's spin is polarized along the x axis of the Bloch sphere. A magnetic field, pointing in the z direction and localized only within the barrier, causes the spin of the particle to precess while inside the barrier. By measuring the precession angle θ_y after the scattering event for either reflected or transmitted particles, the dwell time conditioned on these final states can be extracted from $\tau_y = \theta_y/\omega_L$, where ω_L is the Larmor frequency. In addition to the "in-plane" angle θ_y, an "out-of-plane" angle, θ_z, results from the preferential transmission of the spin component antiparallel to the magnetic field, which experiences an effectively lower barrier due to the magnetic potential energy [26]. Accordingly, a second time $\tau_z = \theta_z/\omega_L$ can be defined.

The meaning of these two times becomes clear by viewing the Larmor clock as a von Neumann measurement [25,27]. The interaction Hamiltonian of the Larmor clock, $H_{\rm int} \sim \boldsymbol{S}\cdot\boldsymbol{B} \sim S_z B_0 \Theta_d$, couples the spin of each particle to the projector onto the barrier region. In this way, the spin acts as the pointer of a measurement apparatus observing whether the system (each particle) is inside the barrier. While S_z, the occupation difference between $|\uparrow\rangle$ and $|\downarrow\rangle$, represents the pointer momentum (i.e., the generator of pointer translations), the conjugate pointer position is the phase difference between $|\uparrow\rangle$ and $|\downarrow\rangle$. Accordingly, we associate τ_y with the time spent inside the barrier and τ_z with the measurement backaction due to the effect of this interaction on the tunneling probability. In the limit of a weak measurement, $B_0 \to 0$, the Larmor times for transmission can be written [26]

$$\tau_y + i\tau_z = -\hbar\frac{\partial\phi}{\partial V_0} + i\hbar\frac{\partial \ln(|t|)}{\partial V_0} = i\hbar\frac{\partial \ln t}{\partial V_0}, \quad (2)$$

where ϕ is the phase of the transmission amplitude t, and V_0 is the energy of the barrier. It turns out that the Larmor times are equivalent to the weak value of the projector Θ_d [25,28].

Figure 1(a) illustrates that a particle with energy E and penetration depth $\kappa^{-1} \propto (V_0 - E)^{-1/2}$ incident on a barrier of height V_0 has a lower probability to be in the forbidden region than the same particle would when incident on a lower energy barrier, V_0'. Hence, the dwell time in the case with the higher barrier is shorter and similarly the dwell time for a fixed barrier height is shorter for particles with less energy. Here, we demonstrate that these trends hold for the Larmor tunneling time τ_y, a fact predicted nearly 40 years ago [26,29]. One might find it reasonable that lower energy particles penetrate less deeply and therefore are *reflected* without spending much time in the barrier. No such argument applies to transmitted particles that traverse the entire barrier.

We implement a Larmor time measurement in a Bose-Einstein condensate of ^{87}Rb atoms. The long wavelengths and slow dynamics of ultracold atoms make tunneling and its timescales convenient for experimental study. Figure 2 illustrates the sequence of our experimental procedure (see the Supplemental Material [30] for further details of advances on previous methods [24]). About 3000 atoms

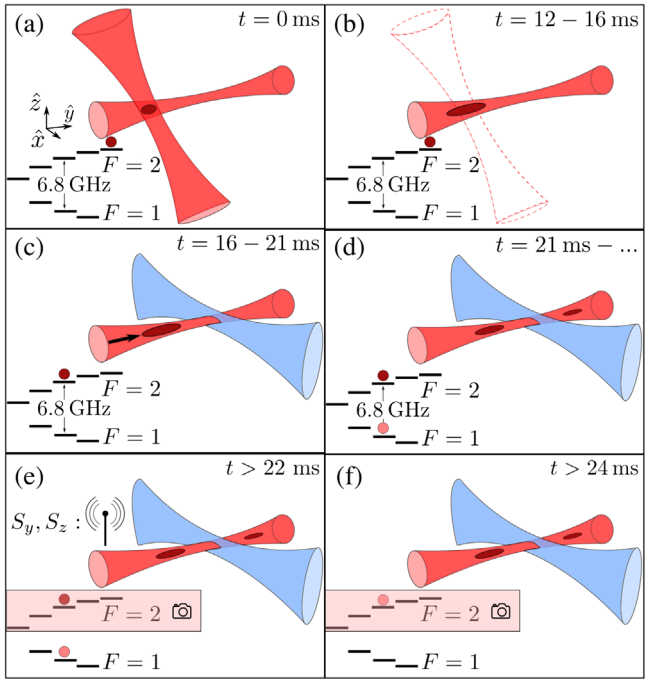

FIG. 2. The experimental procedure. (a) A cloud of ^{87}Rb atoms is condensed in the $|F = 2, m_F = 2\rangle$ state and confined at the intersection of two optical dipole traps, one of which is elongated and forms a quasi-1D system for the collision. (b) Matter-wave lensing prepares an atomic wave packet narrow in momentum. (c) A variable-duration magnetic field gradient pushes the atomic wave packet toward a 421.38 nm optical barrier. Before reaching the barrier, the spins of the atoms are transferred to the $|F = 2, m_F = 0\rangle$ state via ARP. (d) A two-photon Raman transition between the clock states of the hyperfine manifold implements the Larmor measurement during the collision with the barrier. (e),(f) Well after the collision, the $\langle S_x\rangle$, $\langle S_y\rangle$, and $\langle S_z\rangle$ components of the net magnetization vector are obtained by sequential imaging of the hyperfine populations. Measurements of the $\langle S_y\rangle$ and $\langle S_z\rangle$ components are preceded by $\pi/2$ MW rotations about the z and y axes of the Bloch sphere, respectively. ARP transfers the $|F = 1, m_F = 0\rangle$ population to $|F = 2, m_F = 0\rangle$ prior to the second absorption image.

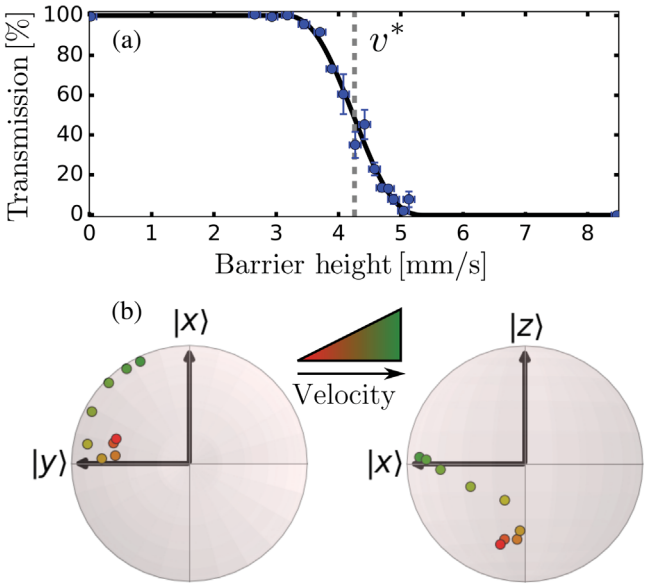

FIG. 3. Typical data from an experimental run. (a) Transmission of a wave packet with average incident velocity v^* through barriers of varying heights measures the width of the incident atomic cloud's velocity distribution. (b) The components of the Bloch vector for the transmitted wave packet are extracted for wave packets with different incident velocities.

are initially [Fig. 2(a)] condensed in the $|F = 2, m_F = 2\rangle$ state of the $5S_{1/2}$ ground orbital of rubidium and confined in a 1054 nm crossed optical dipole trap. An elongated dipole trap forms a quasi-1D waveguide for the scattering event. To construct a wave packet suitably narrow in momentum such that transmission through our barrier has a minimal contribution from classical spilling, we perform matter-wave lensing on the atomic cloud [Fig. 2(b)] and achieve velocity widths close to 0.3 mm/s, corresponding to a thermal de Broglie wavelength of approximately 5 μm. The atoms are "kicked" by the same beam used in the initial crossed optical dipole trap. The resulting velocity spread is measured concurrently with the Larmor experiment using a technique analogous to a knife-edge calibration of an optical beam's transverse extent [31] [Fig. 3(a)]. This technique is also used to calibrate the barrier's height, which is the peak potential energy (or equivalent velocity) of the barrier and equal to the incident energy at which half the atoms are transmitted.

A variable-duration magnetic field gradient pushes the atomic wave packet toward a 421.38 nm beam of light, which acts as a repulsive barrier for the atoms. The barrier intersects the waveguide near the center of its longitudinal potential [Fig. 2(c)]. In this configuration, the wave packet has a single opportunity to tunnel through the barrier. The mean velocity at which the cloud collides with the barrier is extracted from the motion in the absence of the barrier, accounting for the acceleration imparted by the waveguide. Along $\hat{y}$, the barrier has a Gaussian profile with $1/e^2$ radius of 1.3 μm, permitting significant tunneling, while the transverse dimensions, $d_z = 50$ μm and $d_x = 8$ μm, ensure that the atomic wave packet collides with an essentially uniform barrier.

Before reaching the barrier, the atoms are transferred to the $|F = 2, m_F = 0\rangle$ state via an adiabatic rapid passage (ARP) sweep of a radio frequency field. The clock states of the hyperfine manifold serve as an effective spin-1/2 system for the Larmor measurement, where $|F = 2, m_F = 0\rangle \equiv |x\rangle = (|\uparrow\rangle + |\downarrow\rangle)/\sqrt{2}$ and $|F = 1, m_F = 0\rangle \equiv |-x\rangle = (|\uparrow\rangle - |\downarrow\rangle)/\sqrt{2}$, in the notation of Fig. 1. The Larmor probe is implemented using the same beam of light as the barrier. A 6.8 GHz electro-optic modulator performs phase modulation on the light, and an etalon with a FWHM

of 12 GHz filters out unwanted sidebands. Together, the carrier and a single sideband couple the $|\pm x\rangle$ states via a two-photon Raman transition, acting as a pseudomagnetic field pointing along the z axis of the Bloch sphere. A 1 G magnetic field pointing along $-\hat{x}$ sets the quantization axis for the atoms, and the light is circularly polarized to drive $\sigma^+ - \sigma^+$ transitions. We use the rotation angles experienced by high-velocity clouds, which are transmitted classically over the barrier, to calibrate the effective Larmor frequency of the Raman beams.

After the wave packet has left the barrier region, the angles of rotation depicted in Fig. 1 are extracted from spin tomography of the net magnetization vector of the transmitted cloud. $\langle S_x\rangle$ is measured by counting populations in the $|F=2, m_F=0\rangle$ and $|F=1, m_F=0\rangle$ states. To measure $\langle S_y\rangle$ and $\langle S_z\rangle$, we use a $\pi/2$ microwave (MW) pulse to rotate the axis of interest onto the axis given by the spin state populations before imaging [Fig. 2(e)]. The angle of the torque vector in the yz plane about which this rotation occurs is controlled by the phase relationship between the barrier's Larmor rotation and the MW pulse. Before each data run, we calibrate the phase that aligns the torque vector with the y axis of the Bloch sphere by "zeroing" $\langle S_z\rangle$ for a wave packet with velocity well above the barrier height, where transmission is not biased by spin state.

Atoms are counted *in situ* by sequential absorption imaging of the $|F=2, m_F=0\rangle$ and $|F=1, m_F=0\rangle$ populations with resonant light addressing only the $F=2$ manifold [Figs. 2(e) and (f)]. This keeps the atomic density high during imaging, allowing us to reliably count tens of atoms. Atoms in the $F=2$ manifold in the first image heat up due to scattering of resonant light and escape from the waveguide. A MW ARP transfers atoms from the $|F=1, m_F=0\rangle$ to the $|F=2, m_F=0\rangle$ state, immediately after which a second image is taken. This sequence can count relative atom numbers between the images with better than 98% fidelity.

Figure 3 presents data from one experimental run. During each run, we calibrate the width of the atomic cloud's velocity distribution for one choice of mean incident velocity, 4.26 ± 0.06 mm/s, henceforth referred to as v^*. Figure 3(a) shows the transmission of a wave packet with incident velocity v^* through barriers of different heights. The width of this transmission profile is a measure of the atomic cloud's velocity spread (see the Supplemental Material [30] for details of fit function) [31].

The 2D projections of the Bloch sphere in Fig. 3(b) show the rotation angles from a Larmor measurement. We perform constrained maximum-likelihood estimation of the net magnetization vector of transmitted atoms given the raw tomographic data extracted from the absorption images. In addition, we compensate for drifts in the relative phase between the MW pulse and the Larmor rotation, which we monitor throughout the experiment. These drifts typically require us to apply a 10° to 20° rotation to the $\langle S_y\rangle$ and $\langle S_z\rangle$ results. The in-plane angles of rotation for the two fastest incident wave packets are used to determine the Rabi frequency for each run, which always fell in the range 150–350 Hz [with the exception of some of the above-barrier data indicated in the inset of Fig. 4(a)].

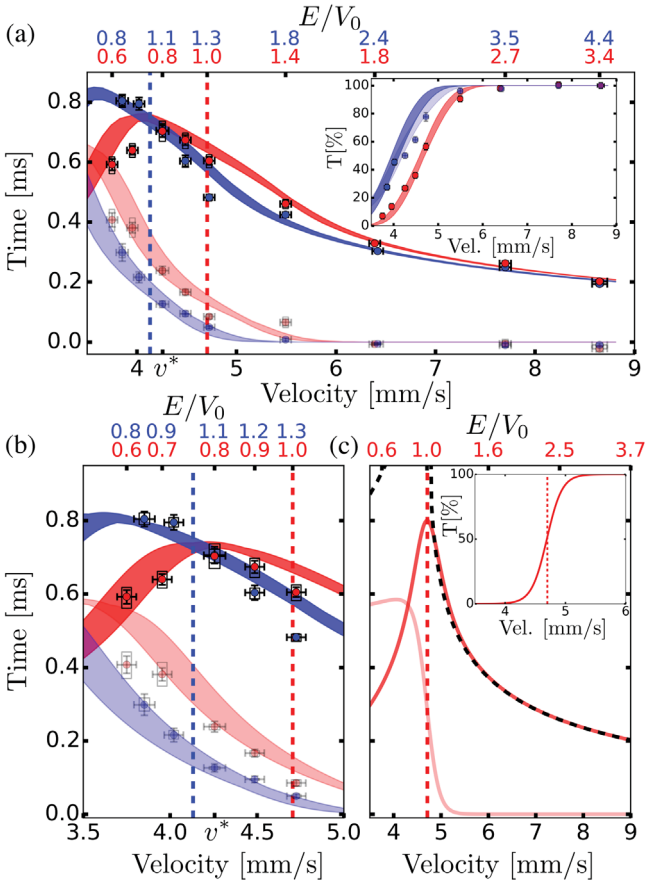

FIG. 4. Larmor times. (a) Measured Larmor times τ_y (solid markers) and $|\tau_z|$ (faded markers) for two different barrier heights, 4.71 ± 0.05 mm/s (red) and 4.13 ± 0.08 mm/s (blue), depicted by the vertical dashed lines, versus incident velocity (lower axis) and normalized energy (upper axis). Statistical and systematic errors are given by the bars and rectangular outlines, respectively, which are sometimes smaller than the markers. Colored bands show GP simulations of the Larmor experiment, bounded by the uncertainties in the measured barrier heights and in the velocity width at v^*. Inset: Experimental and simulated transmission. Some of the above-barrier data for the lower barrier height set had an atypically large Rabi frequency, 808 ± 12 Hz. While this modifies the transmission, indicated by the faded blue markers and bands, it does not significantly affect these times. (b) Low energy data of (a), now compared to weak-value calculations weighted by the inferred velocity profile of the transmitted wave packet. The shaded regions are bounded as in (a). (c) Monochromatic weak-value calculations of the Larmor times (red) for a Gaussian barrier of height 4.71 mm/s and the semiclassical expression [32] used to calibrate the Larmor frequency above the barrier (see the Supplemental Material [30]). Inset: Transmission profile.

Figure 4 presents the Larmor times versus the incident velocity of wave packets colliding with barriers of two different heights: 4.71 ± 0.05 mm/s (red) and 4.13 ± 0.08 mm/s (blue), indicated by the vertical dashed lines. The error bars on the markers represent the rms width of the data's distribution, while the rectangular outlines depict the systematic errors due to the aforementioned compensations to the spin components as well as the uncertainty in the measured Rabi frequency. Below the barrier we observe two important features of the τ_y data: (1) τ_y decreases with decreasing incident energy, a 2σ and 4σ result considering the high-barrier data, and (2) τ_y increases as the barrier height decreases, an 8σ and 6σ result considering the two lowest energies of each set. The opposite behavior is shown by $|\tau_z|$, signifying that the backaction of the measurement increases for higher barriers and lower incident velocities in the measured energy range.

We compare our data to two theoretical calculations. The shaded regions in Fig. 4(a) describe one-dimensional Gross-Pitaevskii (GP) simulations [33] of the Larmor experiment in the presence of the longitudinal potential of the waveguide, matching the measured rms velocity width 0.35 ± 0.03 mm/s at v^*. The regions are bounded by the uncertainty in the measured velocity width and barrier height for each dataset. These simulations model the changing velocity profile of the wave packet resulting from the interplay of the repulsive atomic interactions and the confining potential of the waveguide before atoms reach the barrier (see the Supplemental Material [30] for details). For our experimental parameters, wave packets with slower incident velocities develop smaller velocity widths. The GP simulations explain two key features of our results. A nonzero τ_z appears for velocities above the barrier, contrary to the predictions of the ideal monochromatic theory, due to the portion of the velocity distribution near or just below the barrier height. In addition, we see a significant decrease in τ_y and increase in $|\tau_z|$ for the slowest wave packets, whose velocity profile is narrow enough that transmission is dominated by energies below the barrier. The GP simulations indicate that the rms velocity width of the wave packet drops by 0.06 mm/s, comparing the width inferred from simulations of the slowest incident wave packet and our measured value. In order to find a lower bound for the fraction of atoms that tunneled through the barrier, we use the conservative hypothesis that wave packets slower than v^* had the same velocity width as the measured value.

With this premise, we compare the low-energy data to weak-value calculations of the Larmor times, as given by Eq. (2). Figure 4(c) shows monochromatic calculations with a Gaussian barrier of height 4.71 mm/s, whereas Fig. 4(b) compares the below-barrier data to the average time calculated for the spread of velocities transmitted through both barriers. As before, the shaded regions are bounded by the uncertainties in the measured velocity width and barrier height for each dataset. We observe close agreement between the weak-value calculations and our data as well as with GP simulations. In this experiment, atomic interactions evidently played little role in the transmitted times, and so the association of the data with the conditional dwell time inside the barrier is supported. In contrast, the measured Larmor times for the reflected atoms show differences from the predictions of the noninteracting weak-value theory. We believe that the mean-field energy due to atomic interactions in the high density regions in front of the barrier are important to understanding those data, which will be the topic of forthcoming work.

For the dataset with a higher barrier, we estimate from the measured velocity width that at least 90% of atoms tunneled for the lowest incident energy measured and 65% of the interaction between the Larmor probe and the transmitted wave packet occurred in a forbidden region. For the wave packet incident at v^*, we deduce that 50% of transmitted atoms tunneled through the higher barrier and 20% of the interaction between Larmor probe and transmitted wave packet occurred in a forbidden region. The mean transmitted velocity for this data point is within uncertainty of the height of the barrier, which is consistent with the decrease in τ_y. As shown in Fig. 4(c), in the monochromatic limit τ_y reaches its maximum at the velocity matching the height of a Gaussian barrier and is roughly symmetric for nearby velocities about this peak. Thus, given the symmetry of the transmission profile of a Gaussian barrier (Fig. 4(c) inset) and a smooth incident velocity profile, τ_y is only expected to decrease for energies below the barrier once the energy is low enough that a majority of atoms in fact tunnel through the barrier. Hence, both the measured velocity profile of the transmitted wave packets and the decrease in τ_y are consistent with a majority of atoms having tunneled for the lowest incident energies. This was not observed in [24] given the larger and more uncertain velocity widths there, as well as the omission of some of the systematic effects described here.

The work here shows that tunneling generally takes less time when the tunneling event has a lower probability to occur due to a larger energy deficit below the barrier. We observe the characteristic decrease of τ_y below the barrier, which for a Gaussian barrier indicates that transmission is dominated by tunneling. Additionally, we witness the increase in τ_y for lower barriers and conclude through comparisons with theory that atomic interactions play little role in our measured times in transmission. Future work will study the distinct histories of transmitted and reflected particles, not only due to the role of atomic interactions, but more fundamentally because of the differing forbidden regions these subensembles probe.

The authors would like to thank Kehui Li for improvements to the absorption image analysis, Joseph McGowan, Nick Mantella, and Aharon Brodutch for critical reading of the manuscript, as well as Ramón Ramos and Isabelle

Racicot for experimental developments that culminated in [24]. This work was supported by NSERC and the Fetzer Franklin Fund of the John E. Fetzer Memorial Trust. A. M. S. acknowledges support as a CIFAR Fellow.

*Corresponding author.
dspierin@physics.utoronto.ca
†Also at Canadian Institute for Advanced Research, Toronto, Ontario, Canada.

[1] E. H. Hauge and J. A. Støvneng, Tunneling times: A critical review, Rev. Mod. Phys. **61**, 917 (1989).
[2] R. Landauer and Th. Martin, Barrier interaction time in tunneling, Rev. Mod. Phys. **66**, 217 (1994).
[3] R. Y. Chiao and A. M. Steinberg, Tunneling times and superluminality, Prog. Opt. **37**, 345 (1997).
[4] A. Ranfagni, D. Mugnai, P. Fabeni, and G. Pazzi, Delay-time measurements in narrowed waveguides as a test of tunneling, Appl. Phys. Lett. **58**, 774 (1991).
[5] A. Enders and G. Nimtz, On superluminal barrier traversal, J. Phys. I (France) **2**, 1693 (1992).
[6] A. M. Steinberg, P. G. Kwiat, and R. Y. Chiao, Measurement of the Single-Photon Tunneling Time, Phys. Rev. Lett. **71**, 708 (1993).
[7] C. Spielmann, R. Szipöcs, A. Stingl, and F. Krausz, Tunneling of Optical Pulses through Photonic Band Gaps, Phys. Rev. Lett. **73**, 2308 (1994).
[8] L. Brillouin, *Wave Propagation and Group Velocity*, Vol. 8 (Academic Press, New York, 1960).
[9] P. Eckle, M. Smolarski, P. Schlup, J. Biegert, A. Staudte, M. Schöffler, H. G. Muller, R. Dörner, and U. Keller, Attosecond angular streaking, Nat. Phys. **4**, 565 (2008).
[10] U. S. Sainadh, H. Xu, X. Wang, A. Atia-Tul-Noor, W. C. Wallace, N. Douguet, A. Bray, I. Ivanov, K. Bartschat, A. Kheifets, R. T. Sang, and I. V. Litvinyuk, Attosecond angular streaking and tunnelling time in atomic hydrogen, Nature (London) **568**, 75 (2019).
[11] U. S. Sainadh, R. Sang, and I. Litvinyuk, Attoclock and the quest for tunnelling time in strong-field physics, J. Phys. **2**, 042002 (2020).
[12] A. S. Landsman, M. Weger, J. Maurer, R. Boge, A. Ludwig, S. Heuser, C. Cirelli, L. Gallmann, and U. Keller, Ultrafast resolution of tunneling delay time, Optica **1**, 343 (2014).
[13] N. Camus, E. Yakaboylu, L. Fechner, M. Klaiber, M. Laux, Y. Mi, K. Z. Hatsagortsyan, T. Pfeifer, C. H. Keitel, and R. Moshammer, Experimental Evidence for Quantum Tunneling Time, Phys. Rev. Lett. **119**, 023201 (2017).
[14] A. Fortun, C. Cabrera-Gutiérrez, G. Condon, E. Michon, J. Billy, and D. Guéry-Odelin, Direct Tunneling Delay Time Measurement in an Optical Lattice, Phys. Rev. Lett. **117**, 010401 (2016).
[15] L. Torlina, F. Morales, J. Kaushal, I. Ivanov, A. Kheifets, A. Zielinski, A. Scrinzi, H. G. Muller, S. Sukiasyan, M. Ivanov, and O. Smirnova, Interpreting attoclock measurements of tunnelling times, Nat. Phys. **11**, 503 (2015).
[16] H. Ni, U. Saalmann, and J.-M. Rost, Tunneling Ionization Time Resolved by Backpropagation, Phys. Rev. Lett. **117**, 023002 (2016).
[17] T. Zimmermann, S. Mishra, B. R. Doran, D. F. Gordon, and A. S. Landsman, Tunneling Time and Weak Measurement in Strong Field Ionization, Phys. Rev. Lett. **116**, 233603 (2016).
[18] C. Hofmann, A. S. Landsman, and U. Keller, Attoclock revisited on electron tunnelling time, J. Mod. Opt. **66**, 1052 (2019).
[19] A. I. Baz, Lifetime of intermediate states, Sov. J. Nucl. Phys. **4**, 182 (1966).
[20] V. F. Rybachenko, Time of penetration of a particle through a potential barrier, Sov. J. Nucl. Phys. **5**, 635 (1967).
[21] M. Deutsch and J. E. Golub, Optical larmor clock: Measurement of the photonic tunneling time, Phys. Rev. A **53**, 434 (1996).
[22] P. Balcou and L. Dutriaux, Dual Optical Tunneling Times in Frustrated Total Internal Reflection, Phys. Rev. Lett. **78**, 851 (1997).
[23] M. Hino, N. Achiwa, S. Tasaki, T. Ebisawa, T. Kawai, T. Akiyoshi, and D. Yamazaki, Measurement of Larmor precession angles of tunneling neutrons, Phys. Rev. A **59**, 2261 (1999).
[24] R. Ramos, D. Spierings, I. Racicot, and A. M. Steinberg, Measurement of the time spent by a tunnelling atom within the barrier region, Nature (London) **583**, 529 (2020).
[25] A. M. Steinberg, How Much Time Does a Tunneling Particle Spend in the Barrier Region?, Phys. Rev. Lett. **74**, 2405 (1995).
[26] M. Büttiker, Larmor precession and the traversal time for tunneling, Phys. Rev. B **27**, 6178 (1983).
[27] A. M. Steinberg, Conditional probabilities in quantum theory and the tunneling-time controversy, Phys. Rev. A **52**, 32 (1995).
[28] Y. Aharonov, D. Z. Albert, and L. Vaidman, How the Result of a Measurement of a Component of the Spin of a Spin-1/2 Particle can Turn Out to be 100, Phys. Rev. Lett. **60**, 1351 (1988).
[29] J. P. Falck and E. H. Hauge, Larmor clock reexamined, Phys. Rev. B **38**, 3287 (1988).
[30] See Supplemental Material at http://link.aps.org/supplemental/10.1103/PhysRevLett.127.133001 for details of the experimental procedure, data analysis, and simulations.
[31] R. Ramos, D. Spierings, S. Potnis, and A. M. Steinberg, Atom-optics knife edge: Measuring narrow momentum distributions, Phys. Rev. A **98**, 023611 (2018).
[32] M. Büttiker and R. Landauer, Traversal Time for Tunneling, Phys. Rev. Lett. **49**, 1739 (1982).
[33] W. Bao, D. Jaksch, and P. A. Markowich, Numerical solution of the Gross-Pitaevskii equation for Bose-Einstein condensation, J. Comput. Phys. **187**, 318 (2003).

Correction: The temperature value in the first sentence of the fourth paragraph contained a typographical error and has been replaced.